Available online at www.sciencedirect.com
ScienceDirect
Trans. Nonferrous Met. Soc. China 34(2024) 1178−1190
Transactions of Nonferrous Metals Society of China
www.tnmsc.cn

New model for predicting homogenization kinetics of typical wrought superalloy

Xian-guang ZHANG[1,2], Wen-chao YANG[2], Yang ZHOU[3,4], Jian-hao YAN[2], Dong-ping XIAO[3,4], Lang SHUI[3,4], Jian-hui FU[3,4], Fei SUN[5], Peng SHI[2], Jia-jun CHEN[2], Yi-wu PEI[2], Jian ZHANG[3,4]

1. State Key Laboratory of Advanced Metallurgy, University of Science and Technology Beijing, Beijing 100083, China;
2. School of Metallurgical and Ecological Engineering, University of Science and Technology Beijing, Beijing 100083, China;
3. Chengdu Advanced Metal Materials Industrial Technology Institute Co., Ltd. Chengdu 610300, China;
4. Pangang Group Research Insitute Co., Ltd. Panzhihua 617000, China;
5. Department of Material Design Innovation Engineering, Nagoya University, Furo-cho, Chikusa-ku, Nagoya 464-8603, Japan

Received 24 April 2023; accepted 12 October 2023

Abstract: A new homogenization kinetics prediction model for wrought superalloys based on the concept of diffusion distance was proposed. The micro-segregation and homogenization kinetics of Ni-based wrought superalloy, GH4141, were systematically studied by using the quantitative electron prob X-ray micro-analyzer (EPMA) analyses. There is a discrepancy between the predicted homogenization kinetics by the residual segregation index model and the experimental measurement. Both the experiments and theoretical analyses reveal that the homogenization kinetics can be reasonably predicted by the diffusion distance model under 1D-diffusion condition, with considering the diffusion-direction factor that is usually ignored. The new model provides a new option for predicting the homogenization kinetics with only necessarily knowing the original dendrite arm spacing and diffusion coefficient.
Key words: wrought superalloy; micro-segregation; homogenization kinetics; prediction model; diffusion distance

1 Introduction

Wrought superalloy is widely used in aerospace engines due to its excellent oxidation resistance, corrosion resistance and structure stability at high temperatures [1−5]. The wrought superalloy is fabricated through traditional casting and forging processes. The micro-segregation of alloying elements and undesirable phase precipitation inevitably occur during the solidification process [6−8], which have seriously detrimental effects on the services performance or formability of wrought superalloy [9−12]. Therefore, homogenization is necessarily conducted to eliminate the element segregation and redissolve the precipitates.

As for the wrought superalloy, the homogenization treatment is usually performed at temperatures above the γ' solution temperature, while below the incipient melting point [13−16]. This temperature range is named the "homogenization temperature window". Currently, the homogenization conditions for most wrought superalloys are generally determined by experience or referenced from the homogenization condition of widely produced Inconel 718 superalloy in the industry [17−19]. For the Ni-based 718Plus

Corresponding author: Xian-guang ZHANG, Tel: +86-10-62332265, E-mail: xgzhang@ustb.edu.cn;
Jian ZHANG, Tel: +86-812-3380508, E-mail: xiaojian529@gmail.com
DOI: 10.1016/S1003-6326(24)66462-9

superalloy, it takes 70 h at 1403 K, or it takes 40 h at 1443 K [20]. Reasonable homogenization parameters are crucial to ensuring high working efficiency and cost-saving for the industry.

Establishing a reliable and easily applied prediction model is a key issue to provide reasonable homogenization parameters for the homogenization treatment of superalloys. Several methods were proposed to predict the homogenization kinetics of superalloy, such as diffusion-controlled transformations (DICTRA) software based on the initially predicted as-cast segregation [21], phase field modeling [22], and residual segregation index (RSI) model [23,24]. Among them, the RSI model is most frequently used, although the accuracy of it has not been fully verified yet. Indeed, the RSI model was mainly used for determining the diffusion coefficient based on the direct experimental measurement of the change in RSI [25−27]. Furthermore, there is a dispute on the criteria for determining the degree of homogenization when using the RSI model [9,27], which makes it more difficult to be applied. In addition, the prediction methods based on the modelling or software are not readily to be applied in general or largely depended on the initially predicted reliability of segregation. Therefore, it is urgent to establish a more reliable and easily applied model for predicting the homogenization kinetics of superalloy.

In response to the above existing problems in homogenization prediction, the present work proposed a new model for predicting the homogenization kinetics based on the concept of diffusion distance. The physical process of homogenization is diffusion of segregated elements from high-concentration regions to low-concentration regions making them distribute uniformly [28]. The segregated alloying elements are able to diffuse uniformly, when the elements can diffuse as far as half of dendrite arm spacing. Moreover, the diffusion distance based on Brownian motion theory can be derived accordingly [29]. Therefore, it is possible to apply the diffusion-distance as a new model to predict the element diffusion during the homogenization. This may provide a simple way or new option for predicting the homogenization kinetics. The present study has been undertaken to investigate the possibility of predicting the homogenization kinetics of wrought superalloy by using the concept of diffusion distance through experiments and theoretical analyses.

2 Experimental procedures and thermodynamics analyses

2.1 Experimental procedures

A typical nickel-based superalloy, GH4141, was used in the present study, and the composition of the superalloy is given in Table 1. The as-cast ingot (*d*250 mm) was prepared by the triple-smelting process (vacuum induction melting (VIM), electroslag remelting (ESR), and vacuum arc remelting (VAR)). Samples with the size of 10 mm × 8 mm × 5 mm were cut from the core of the ingot, at which the micro-segregation is most serious and difficult to be homogenized. Homogenization treatments were carried out in a chamber of electric furnace at certain temperatures for various periods. After the homogenization treatment, the specimens were quenched into oil to avoid re-precipitation of other phases.

Table 1 Chemical composition of superalloy used in present study (wt.%)

Cr	Co	Mo	Ti+Al	B	C	Ni
19.58	11.35	10.40	4.50	0.019	0.02	Bal.

Then, the as-cast or homogenized specimens were cut and mechanically polished. After grinding and polishing, the samples were etched with the solution of 8 g $CuSO_4$ + 40 mL HCl + 40 mL C_2H_5OH for revealing the dendrite structure. Microstructural characterizations were conducted by optical microscopy (OM) and field emission scanning electron microscope (FE-SEM, JSM−6701F), operated at 20 kV. The local alloying element distributions were quantitatively analyzed by point analyses based on the standard sample or qualitative mapping by using electron prob X-ray micro-analyzer (EPMA, JXA−8530F Plus), operated at 20 kV. Equally spaced point analyses were used to get the element distribution in the dendrite and inter-dendritic regions, as schematically shown in Fig. 1. Then, the element segregation coefficient, K [30], was obtained.

The grain structures of the as-cast ingot were characterized by electron backscatter diffraction (EBSD, MIRA3 LMH) analyses, operated at 20 kV.

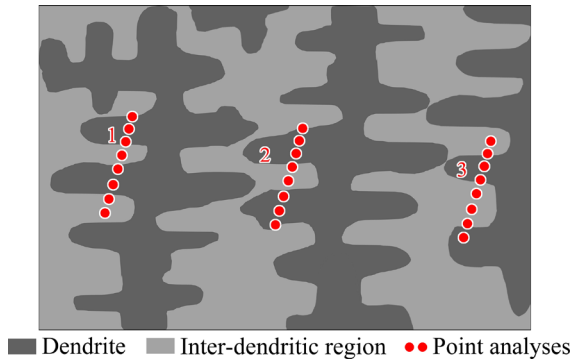

Fig. 1 Schematic illustration of quantitative measurement on local alloying element distributions in as-cast structure for superalloy

The samples were electropolished in the solution of 20 mL HCl + 80 mL C_2H_5OH at the voltage of 20 V to remove the damaged surface before the EBSD analyses.

The element diffusion coefficients of the Ni-based superalloy used in the present study were exported from the diffusion module (DICTRA) of Thermo-Calc software (for simulation of diffusion-controlled reactions of multicomponent alloys) using the TCNI9-MOBNI5 database by considering the wrought superalloy composition in the present study.

2.2 Thermodynamics analyses

Homogenization is applied to dissolving the precipitates for obtaining single γ phase, and making the segregated alloying elements distribute uniformly. The homogenization treatment is generally performed at high temperatures for dozens of hours, which is close to the equilibrium state. Therefore, the equilibrium phase diagram is an important reference for determining the homogenization temperature window.

The calculated equilibrium phase-diagram by using the Jmatpro (V.9.0) is shown in Fig. 2(a). To reveal all the phases clearly, the square regions marked by the broken line in Fig. 2(a) is enlarged and displayed in Fig. 2(b). The γ' dissolution temperature and liquidus temperature are determined to be 1324 and 1516 K, respectively.

The solidification is a non-equilibrium process, and in order to understand the possible phases existing in the as-cast ingot, the non-equilibrium

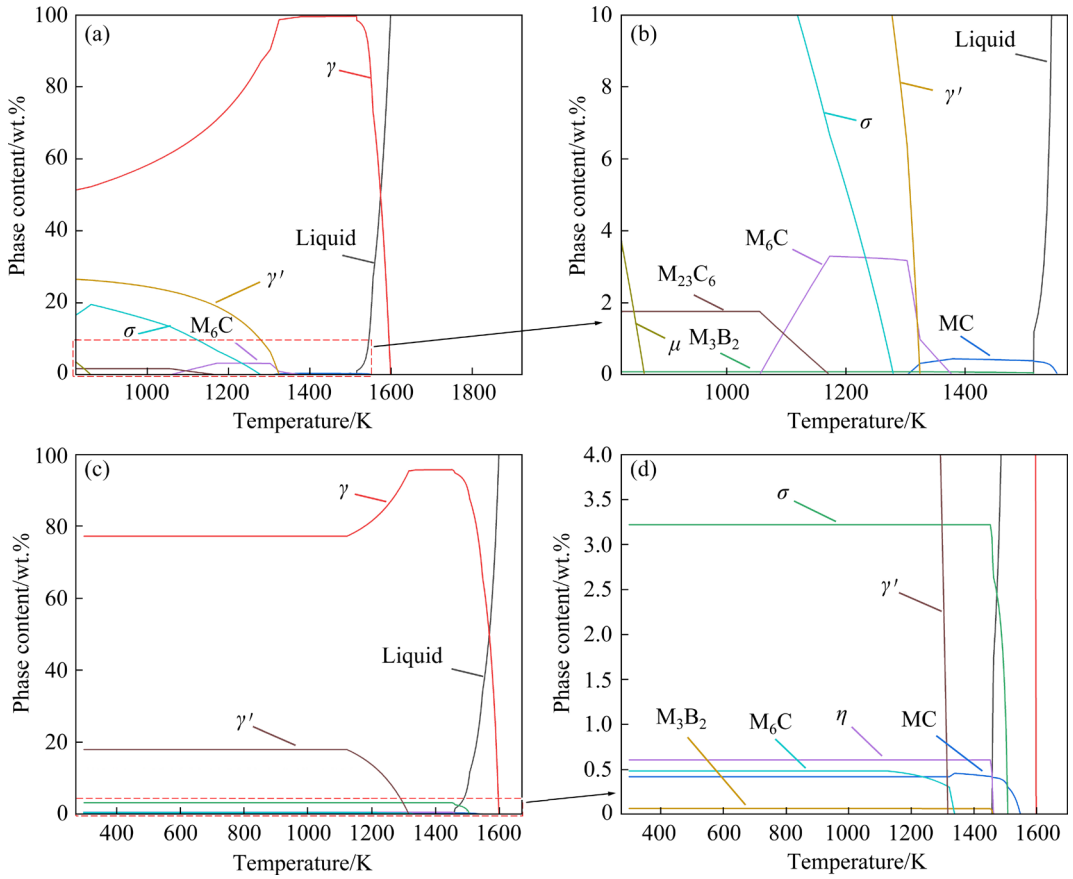

Fig. 2 Equilibrium phase diagram (a) and partially enlarged diagram of marked region (b); Non-equilibrium phase diagram during solidification process (c) and partially enlarged diagram of marked region (d) for superalloy

phase-diagram for the solidification process was calculated, as displayed in Figs. 2(c, d). The precipitates including MC, M_6C, σ, M_3B_2 and η are expected to exist in the as-cast ingot according to Figs. 2(c, d).

The equilibrium dissolution temperature of these precipitates during the homogenization treatment, however, should be determined by using the equilibrium phase diagram shown in Fig. 2(a). According to Figs. 2(a, b), most of the precipitates except MC can be fully dissolved below the liquidus, and the equilibrium dissolution temperature of MC is 1555 K, which is about 40 K above the liquidus. This indicates that the MC may be very difficult to fully dissolve by the homogenization treatment. Therefore, the temperature window for the homogenization treatment is initially determined to be 1378−1516 K, according to the above thermodynamic analyses.

3 Result and discussion

3.1 Quantitative characterization of dendrite structure and micro-segregation

The OM and SEM images of the as-cast ingot are shown in Figs. 3(a) and 3(b), respectively. The typical dendritic structures are clearly observed. The dendrite exhibits light contrast under the OM, while dark under the SEM observations. The secondary dendrite arm spacing (SDAS) was measured by the intercept method and the corresponding result is summarized in Fig. 4. It exhibits a typical normal distribution with the average value of 100.63 μm.

In addition, there are no obvious grain boundaries or grains that could be revealed in the as-cast structure after etching (Fig. 3(a)). In order to reveal the grain structure of the as-cast ingot, EBSD analyses were performed. The OM image taken at higher magnification and the corresponding inverse pole figure (IPF) of the same area analyzed by EBSD are shown in Figs. 3(c) and 3(d), respectively. On the OM observation, obvious dendritic structure is observed; nevertheless, the grains or the grain boundaries are clearly presented in Fig. 3(d), with the grain size around hundreds of microns. Multiple ‘dendrites’ exist within one single grain, and the chemically etched dendrite does not real structures physically existing in the as-cast ingot.

The local alloying element distributions in the as-cast ingot were analyzed by EPMA. The SEM image and the element distributions in the same area are shown in Fig. 5. The alloying elements including Al, Co, Cr and Ni are enriched in the dendrites, while Mo and Ti are enriched in inter-dendritic regions. In addition, it is obvious that the

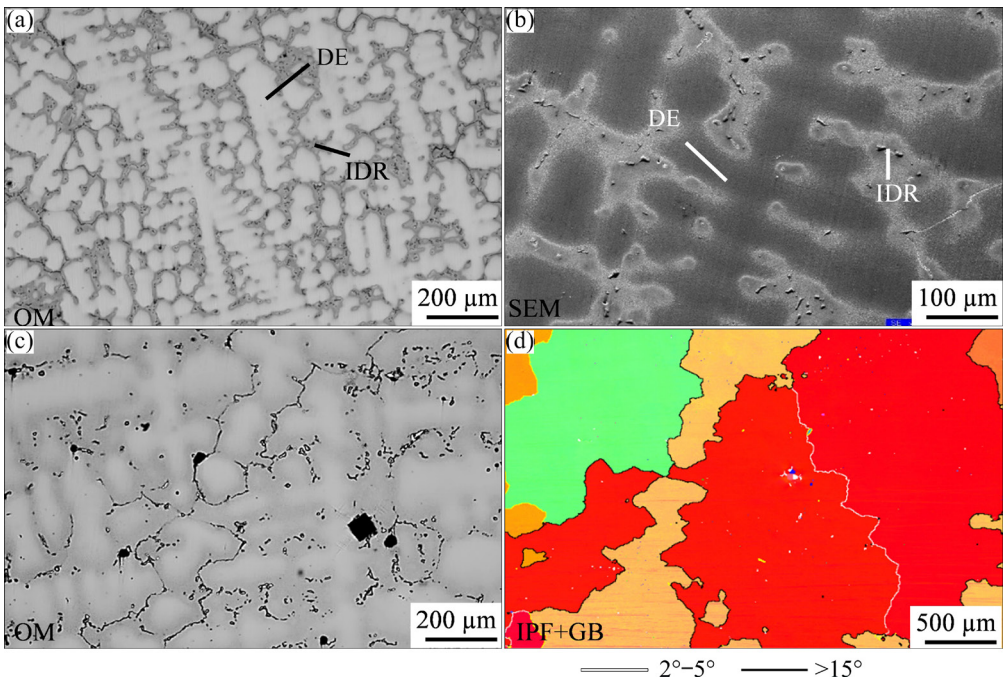

Fig. 3 OM (a) and SEM (b) images of as-cast ingot after chemical etching; OM (c) and inverse pole figure (IPF) map (d) of same area analyzed by EBSD (DE: Dendrite; IDR: Inter-dendritic region)

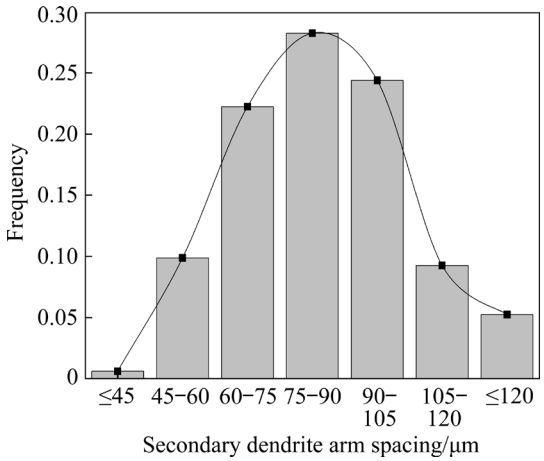

Fig. 4 Quantified secondary dendrite arm spacing distribution

element distribution patterns and the dendritic structures under the SEM observations (Fig. 5(g)) are well matched. This strongly indicates that the etched dendritic 'structure' is the etching contrast caused by uneven distribution of the alloying elements (Figs. 5(a−f)).

The SEM image and the quantitatively analyzed element distributions along the line shown in the SEM image are displayed in Fig. 6. Al, Co, Cr and Ni are enriched in the dendrites, while Mo and Ti are enriched in inter-dendritic regions. The element distribution is close to sinusoidal function. The segregation coefficient, K, is calculated by Eq. (1) [31]:

$$K=\frac{C_{\text{inter-dendrite}}}{C_{\text{dendrite}}} \tag{1}$$

where $C_{\text{inter-dendrite}}$ and C_{dendrite} are the average alloying element concentrations in the inter-dendritic and dendrite regions, respectively. The calculated K is shown in Fig. 6(h). The Mo and Ti are the strong positively-segregated elements, while the Al and Co are the strong negatively- segregated elements.

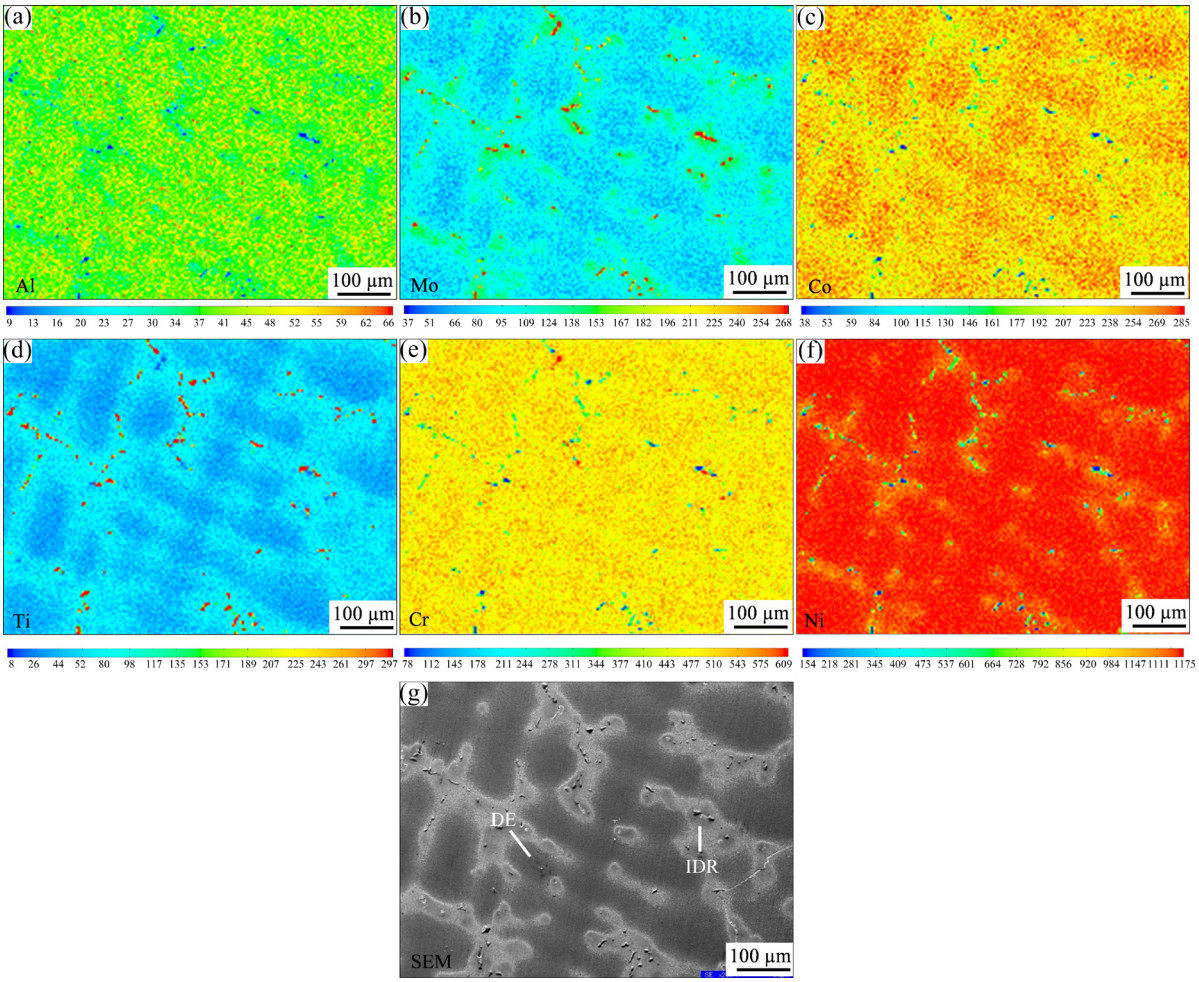

Fig. 5 Alloying element distributions of Al (a), Mo (b), Co (c), Ti (d), Cr (e), and Ni (f) in as-cast ingot of same area with SEM image (g) for superalloy analyzed by EPMA (DE: Dendrite; IDR: Inter-dendritic region)

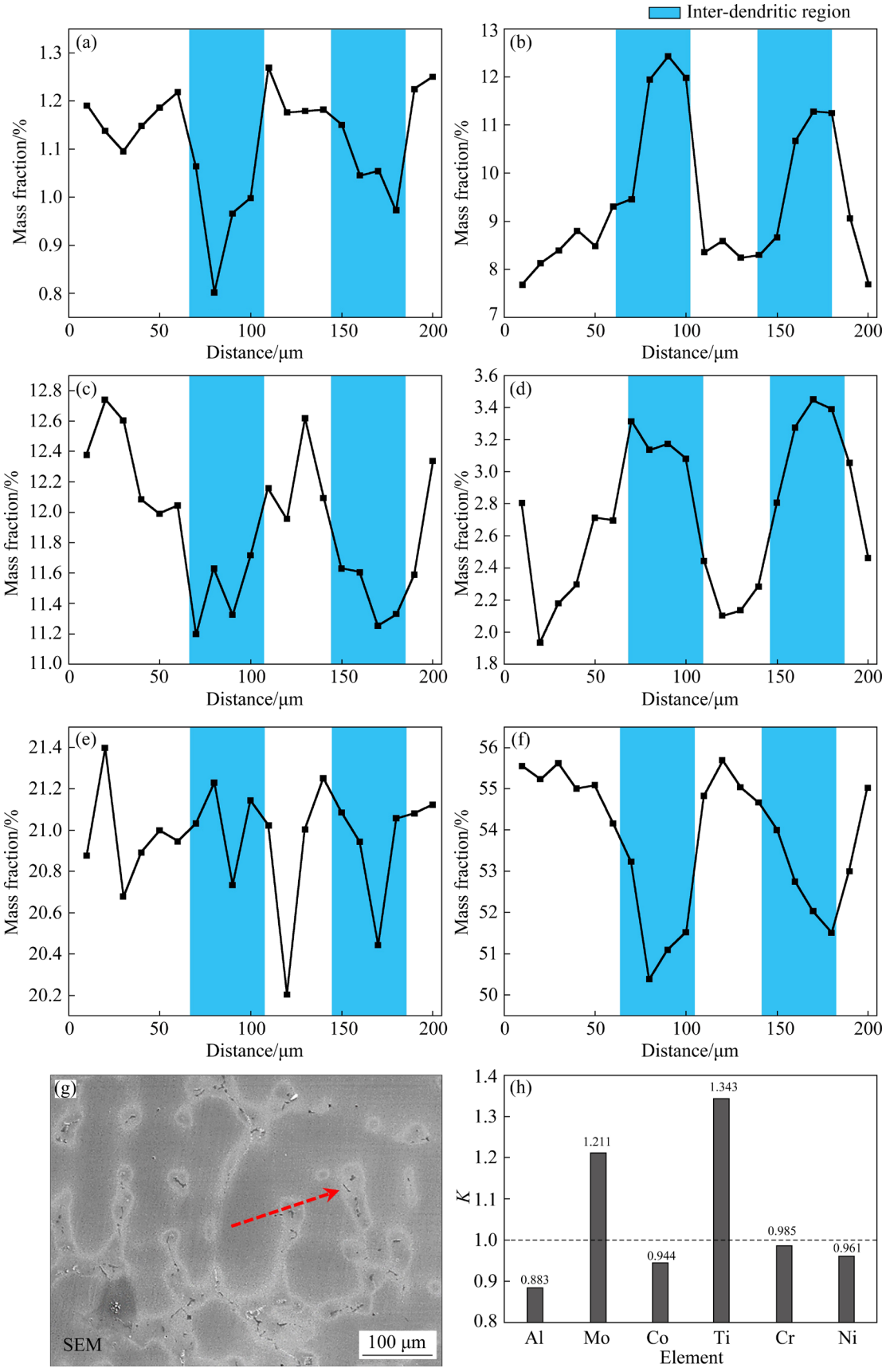

Fig. 6 Quantitatively analyzed element distributions of Al (a), Mo (b), Co (c), Ti (d), Cr (e) and Ni (f) along line in SEM image (g) in as-cast ingot by EPMA, and experimentally measured segregation coefficient K (h)

3.2 Prediction and experimental measurement on homogenization kinetics

In the previous studies, the residual segregation index, δ, was proposed to evaluate the alloying element distribution homogeneity after the homogenization, which is expressed as [31,32]:

$$\delta=\frac{\left(C_{\max}^{t}-C_{\min}^{t}\right)}{\left(C_{\max}^{0}-C_{\min}^{0}\right)} \tag{2}$$

where $C_{\max}^{0}$ and $C_{\min}^{0}$ represent the maximum and minimum concentrations of the alloying elements within the dendrite in the as-cast ingot before homogenization, respectively, and $C_{\max}^{t}$ and $C_{\min}^{t}$ represent maximum and minimum concentrations of the alloying elements after homogenization for time t, respectively.

Considering the sinusoidal function based on the Fick's second law of diffusion during homogenization, the relationship between δ and homogenization time is expressed as follows [9,31]:

$$\ln\delta=\frac{-4\pi^2}{L^2}Dt \tag{3}$$

where L and D present the SDAS, and element diffusion coefficient, respectively.

The element diffusion coefficient (D) is expressed in Eq. (4) [30,31]:

$$D=D_0\exp\left(\frac{-Q}{RT}\right) \tag{4}$$

where D_0, Q and T represent the diffusion constant, diffusion activation energy and temperature, respectively. R is molar gas constant (8.314 J/(mol·K)). Therefore, the diffusion coefficient D is a function of temperature T. According to Eqs. (3) and (4), the residual segregation index, δ, can be written as

$$\ln\delta=\frac{-4\pi^2}{L^2}D_0\exp\left(\frac{-Q}{RT}\right)t \tag{5}$$

According to Eq. (5), δ is a function of t and T. Therefore, δ can be predicted by the known D_0, Q and L. The value of δ is equal to 1 in the initial as-cast ingot and equal to 0 after complete homogenization with uniform element distribution. In general, it is considered that the homogenization is complete when δ is less than 0.2 [27,33−35].

In order to obtain the suggested homogenization conditions by using Eq. (5), the diffusion constant of the main alloying elements (D_0) and diffusion activation energy (Q) were exported from the DICTRA mobility database, which is widely accepted and acknowledged, and the corresponding results of D_0 and Q are summarized in Table 2.

Table 2 Fitted diffusion activation energy Q and diffusion constant D_0 of main alloying elements for superalloy

Element	Q/(10^5J·mol^{-1})	D_0/(10^{-4}m^2·s^{-1})
Al	2.586	1.243
Mo	2.869	1.602
Co	2.768	1.553
Ti	2.569	0.968
Cr	2.785	1.996

The predicted changes in δ by Eq. (5) against the homogenization time within the temperature range of 1378−1516 K, for the main segregated elements are summarized in Fig. 7. The predicted δ values for the Al and Ti decrease very rapidly in the initial stage and approach to 0 after homogenization for 10 h above 1403 K (Figs. 7(a, d)). However, Cr and Co are relatively difficult to diffuse uniformly, which takes 20 h above 1463 K making the δ lower than 0.2. On the other hand, Mo is the most difficult to diffuse uniformly, which takes 50 h at 1403 K and 1433 K, and 20 h above 1463 K. Therefore, 1483 K is selected for the homogenization experiment according to the predictions for ensuring the high homogenization efficiency.

The experimentally measured changes in δ against homogenization time at 1483 K based on the quantitative EPMA analyses, for the Mo, Co, and Ti are shown in Fig. 8. It is obvious that the measured δ values for them are close to 0.2 after homogenization at 1483 K for 20 h or longer, which indicates that the segregated elements diffuse uniformly. It should be pointed out that there is slight increase in δ for Mo and Ti with the increase of annealing time from 20 to 50 h, which belongs to the normal fluctuation of δ due to the slight differences in the degrees of micro-segregation among different samples and areas used for the measurement.

3.3 New prediction model based on diffusion distance

The comparisons in changes of δ against annealing time at 1483 K between the predictions

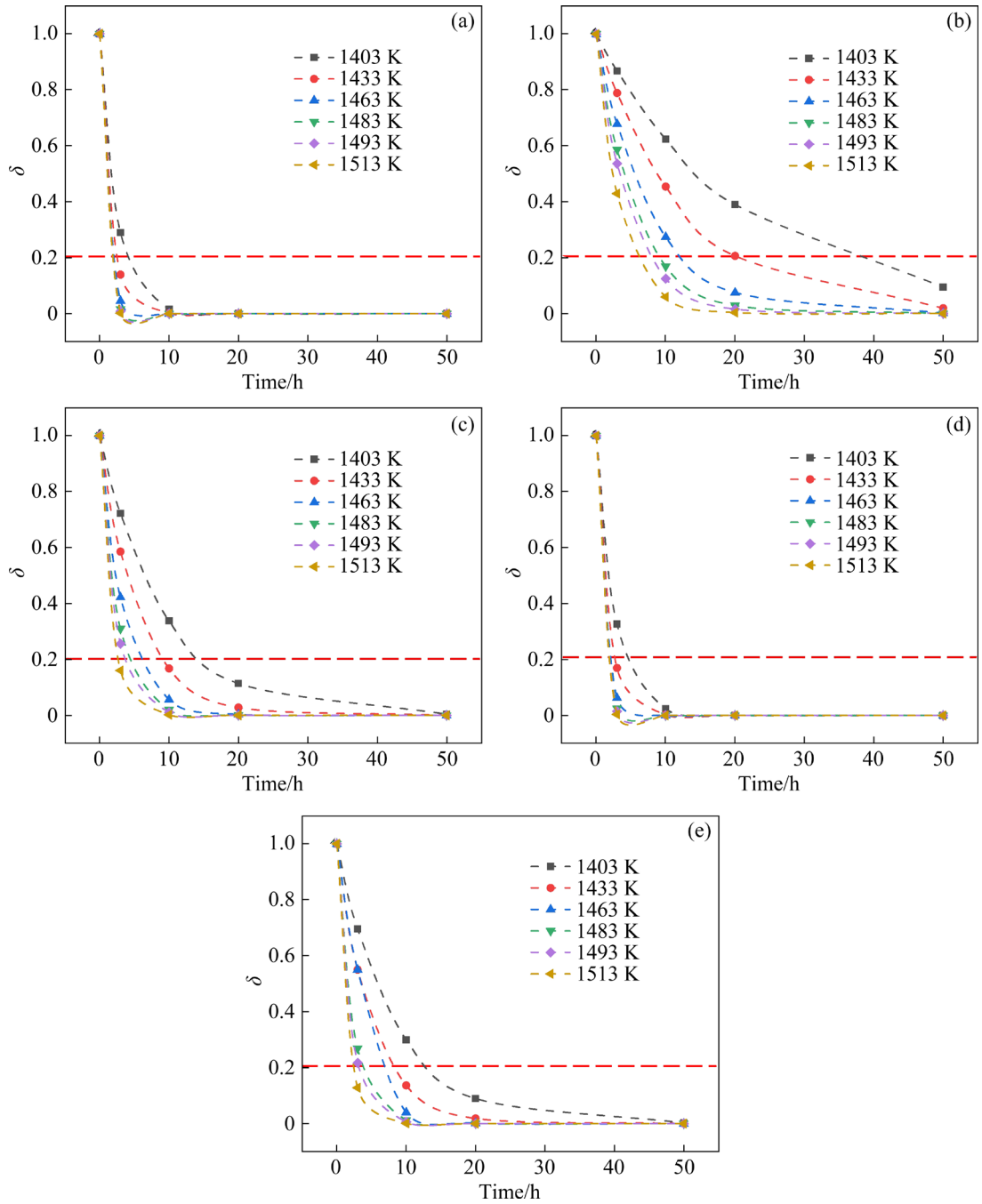

Fig. 7 Predicted changes in residual segregation index, δ, for main alloying elements of Al (a), Mo (b), Co (c), Ti (d) and Cr (e) against homogenization time at different temperatures by residual segregation index model (It is considered that the homogenization is completed, when δ is lower than 0.2)

and measurements are shown in Figs. 9(a, b) by taking the typical segregated alloying elements of Mo and Ti as an example. It is obvious that there are large deviations between the predictions and the measurements for both cases. The predicted δ became lower than 0.2 after homogenization at 1483 K for 10 h, and reached 0 after longer time annealing. In other words, the homogenization is predicted to be completed after homogenization at 1483 K for 10 h. However, the experimental results show that the δ just became close to 0.2 after homogenization at 1483 K for 20 h or longer for both Mo and Ti. Therefore, the prediction by using the residual segregation index (RSI) model cannot ensure the complete homogenization of the segregated alloying elements.

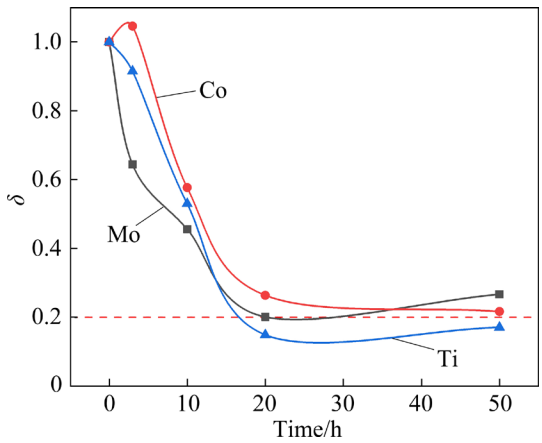

Fig. 8 Experimentally measured changes in residual segregation index, δ, against homogenization time at 1483 K

As stated, the physical process of homogenization is a diffusion of the segregated alloying elements from high concentration regions to low concentration ones, making them distribute uniformly [27]. In the case of as-cast superalloy, the positively segregated elements diffuse from the original inter-dendrite regions to the dendrite regions driven by the element concentration gradient, while the negatively segregated elements diffuse inversely. Thus, the segregated alloying elements can be regarded to diffuse uniformly, when the elements can diffuse as far as half of the SADS. Therefore, it is possible to apply the element diffusion distance as a new model to predict the element diffusion during the homogenization.

According to the literature [26], the diffusion distance, x, is expressed as

$$x=\sqrt{Dt} \tag{6}$$

where D is the diffusion coefficient. In the previous report [32], this model was mainly used for predicting a new homogenization condition based on an experimentally determined homogenization condition for the wrought superalloys. Recently, this model was used for predicting homogenization

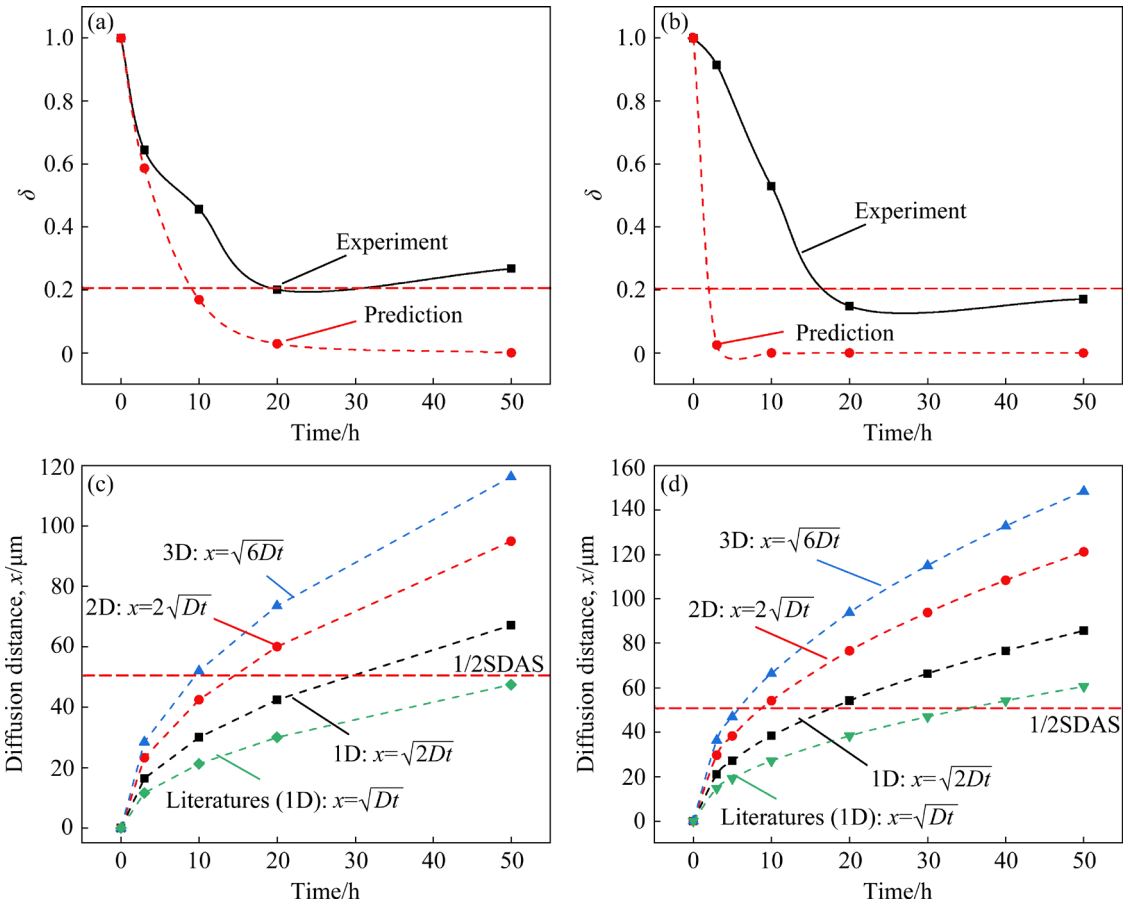

Fig. 9 Comparisons in experimentally measured residual segregation index, δ, and prediction by residual segregation index model for Mo (a) and Ti (b), and calculated diffusion distance, x, at different diffusion dimensions using various diffusion direction factor, k, and literatures by ignoring k, for Mo (c) and Ti (d), in homogenization at 1483 K

time [36]. However, there should be a diffusion-direction factor (k) in the formula, which was usually ignored [32,34,35].

This model is based on the Brownian motion theory and derived by Einstein, and the factor k is equal to $2^{1/2}$ under the 1D diffusion condition [29]. It is supposed that there are two regions with a plan distance of x, with the atomic concentrations of C and $C+(\mathrm{d}C/\mathrm{d}x)x$, respectively. In the case of 1D diffusion, the direction number is 2. Therefore, the plane of unit area diffusion flux, F, for time t can be written as

$$F=-\frac{x}{2t}C+\frac{x}{2t}\left(C+\frac{\mathrm{d}C}{\mathrm{d}x}x\right) \tag{7}$$

Then,

$$F=\frac{x^2}{2t}\frac{\mathrm{d}C}{\mathrm{d}x} \tag{8}$$

According to the definition of diffusion coefficient, under the 1D diffusion condition, the element diffusion distance, x, can be written as

$$x=\sqrt{2Dt} \tag{9}$$

By geometric derivation, k is equal to 2 or $6^{1/2}$ under the 2D or 3D diffusion, respectively [37]. By substitution D with Eq. (4), the diffusion distance, x, can be expressed as follows:

$$x=k\sqrt{\left(D_0\exp\left(\frac{-Q}{RT}\right)\right)t} \tag{10}$$

According to Eq. (10), the diffusion distance x can be predicted at given homogenization time and temperature. Figures 9(c, d) show the calculated diffusion distance x by using various k values as a function of homogenization time at 1483 K for Mo and Ti, respectively. The 3D and 2D predictions are over-estimated in comparison with the measurements for both cases, as shown in Figs. 9(a, b). It takes less than 15 or 10 h to reach the diffusion distance of half SDAS for Mo or Ti, respectively; that is to say, the homogenization is completed within 15 or 10 h for them. However, 20 h is needed according to the experimental results in Fig. 9(a). Therefore, the 2D or 3D prediction cannot ensure the completion of homogenization.

On the other hand, the predictions by using the model of the literatures ignoring the diffusion-direction factor k, are strongly deviated from the measurements as well, which takes around 50 or 40 h for the complete homogenization of Mo or Ti, respectively. The 1D diffusion model predictions with considering the diffusion-direction factor k in Figs. 9(c, d) are reasonable and close to the experimental results, which takes around 27 h for Mo or 18 h for Ti to diffuse up to half SDAS at 1483 K. Hence, the 1D prediction can ensure the complete homogenization with acceptable accuracy.

The diffusion distance model is based on the Brownian motion, which is derived from the point source diffusion model, as shown in Fig. 10. In the 1D diffusion condition, the elements have two diffusion directions, viz., the positive and the negative directions of x-axis, and the diffusion direction factor k is equal to $2^{1/2}$. Under the 2D diffusion, the element in the point source model has four diffusion directions, and the k is equal to 2 according to the vector computation. Similarly, under the 3D diffusion, it has six diffusion directions and the k is equal to $6^{1/2}$ accordingly.

The element diffusion is driven by the element concentration gradient. The segregated alloying element distribution in the as-cast ingot is inherited from the 3D dendritic structure. The original dendrite arm can be regarded as a combination of infinite point sources, and the diffusion of elements along the dendrite stems with almost the same concentration is negligible. Therefore, the 3D

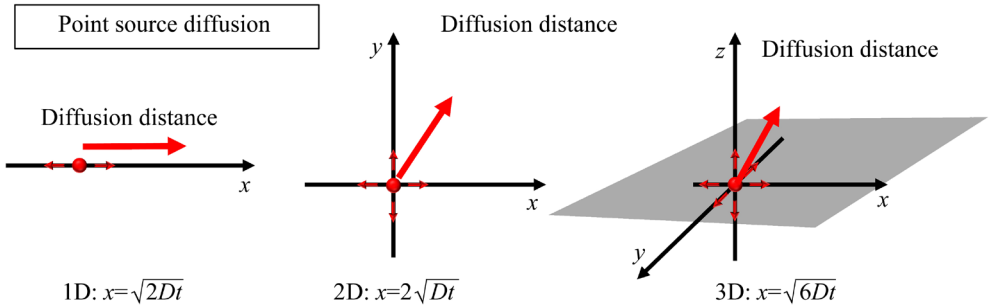

Fig. 10 Schematic illustrations of point source diffusion in 1D, 2D and 3D dimensions

diffusion in the dendrite structure can be simplified to 2D diffusion, as shown in Fig. 11. Then, it can be further simplified to 1D diffusion between adjacent dendrite arms driven by the element concentration gradient. This is well supported by the evidence that secondary dendrite arms are the main segregated units according to Fig. 5. Therefore, 1D diffusion can give a better prediction according to the above discussion.

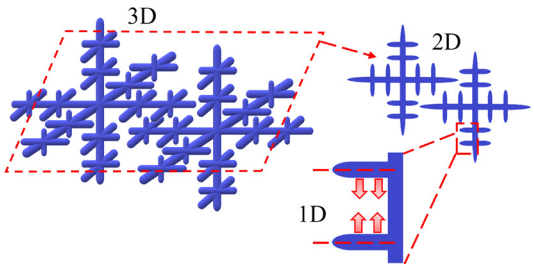

Fig. 11 Schematic illustrations for simplifying of diffusion during homogenization by 1D diffusion model

According to the above analyses using the homogenization kinetics of wrought superalloy GH4141 as an example, the prediction model based on the diffusion distance under the 1D-diffusion with considering the diffusion-direction factor can be applied as a new model to predict the homogenization kinetics. The wrought superalloys are fabricated by general casting method, which has the same characters of the dendrite formation and inter-dendritic segregation during the solidification. The segregated elements diffuse from the high-concentration regions, viz., the original dendrite or inter-dendrite regions, to low-concentration regions during the homogenization. Therefore, this new model based on the diffusion distance is applicable for other wrought superalloys as well. This model is reliable to be applied with only necessarily measuring the original SDAS of the as-cast ingot and using the diffusion coefficient exported from the DICTRA mobility database, which can provide reasonable parameters for the homogenization of wrought superalloys.

4 Conclusions

(1) The Mo and Ti are the strong positively-segregated elements, while the Al and Co are the strong negatively-segregated elements for the GH4141 wrought superalloy. The chemically etched dendrite contrast in the as-cast ingot is the trace of non-uniform alloying element distribution revealed by selective etching, which is not the real structure physically existing in the as-cast ingot.

(2) There is a discrepancy between the predicted homogenization kinetics by the residual segregation index model and the measurement. The prediction by using the residual segregation index model cannot ensure the complete homogenization of the wrought superalloy.

(3) The homogenization kinetics can be reasonably predicted by the new model based on the diffusion distance under 1D-diffusion condition, with considering the diffusion-direction factor which is usually ignored. The prediction model is reliable to be applied with only necessarily measuring the original SDAS of the as-cast ingot and using the diffusion coefficient exported from the DICTRA mobility database.

CRediT authorship contribution statement

Xian-guang ZHANG: Conceptualization, Methodology, Writing − Review & editing, Supervision, Funding acquisition; **Wen-chao YANG:** Methodology, Investigation, Writing − Original draft; **Yang ZHOU:** Resources, Writing − Original draft; **Jian-hao YAN:** Writing − Review & editing; **Dong-ping XIAO:** Writing – Review & editing; **Lang SHUI:** Investigation; **Jian-hui FU:** Investigation; **Fei SUN:** Writing − Review & editing; **Peng SHI:** Investigation; **Jia-jun CHEN:** Investigation; **Yi-wu PEI:** Investigation; **Jian ZHANG:** Investigation, Writing − Review & editing.

Declaration of competing interest

The authors declare that they have no known competing financial interests or personal relationships that could have appeared to influence the work reported in this paper.

Acknowledgments

This research was financially supported by the National Natural Science Foundation of China (No. 51804232), and Beijing Municipal Natural Science Foundation, China (No. 2212041). This work was partially supported by the Interdisciplinary Research Project for Young Teachers of USTB, China (Fundamental Research Funds for the Central Universities, China) (No. FRF-IDRY-20-020).

References

[1] SAHITHYA K, BALASUNDAR I, PANT P, RAGHU T. Comparative study on the high temperature deformation behavior of an as-cast Ni base superalloy subjected to different cooling rates after homogenization [J]. Journal of Alloys and Compounds, 2020, 849: 156626.

[2] ZHANG Heng, LIU Yuan, CHEN Xiang, Zhang Hua-wei, LI Yan-xiang. Microstructural homogenization and high-temperature cyclic oxidation behavior of a Ni-based superalloy with high-Cr content [J]. Journal of Alloys and Compounds, 2017, 727: 410−418.

[3] SAHITHYA K, BALASUNDAR I, PANT P, RAGHU T. Primary hot working characteristics of an as-cast and homogenized nickel base superalloy DMR-742 in the sub and super-solvus temperature regime [J]. Journal of Alloys and Compounds, 2020, 821: 153455.

[4] ZHANG Xian-guang, CHEN Jia-jun, ZHOU Yang, LANG Shui, XIAO Dong-ping, FU Jian-hui, YANG Wen-chao, LIU Huan, REN Ying-jie, SHI Peng, ZAHNG Jian. Oxidation and internal nitridation behaviors of a Ni-based superalloy Rene 65 during high-temperature homogenization [J]. Journal of Iron and Steel Research International, 2023, 30: 1622−1632.

[5] JIANAG Ju-fu, XIAO Guan-fei, WANG Ying, LIU Ying-ze, ZHANG Ying. High temperature deformation behavior and microstructure evolution of wrought nickel-based superalloy GH4037 in solid and semi-solid states [J]. Transactions of Nonferrous Metals Society of China, 2020, 30: 710−726.

[6] CUI Hong-yang, TAN Yi, BAI Ru-sheng, LI Yi, ZHUANG Xin-peng, CHEN Zi-ang, YOU Xiao-gang, LI Peng-ting, CUI Chuan-yong. Microsegregation of new Ni−Co-based superalloy prepared by electron beam smelting layered solidification technology and its homogenization behavior [J]. Materials Characterization, 2022, 184: 111668.

[7] JIANG He, XIANG Xue-mei, DONG Jian-xin. The morphology and characteristics evolution of MC carbide during homogenization in hard-to-deform superalloy GH4975 [J]. Journal of Alloys and Compounds, 2022, 929: 167086.

[8] HAO Jian-qiao, QIN Shu-yang, YAN Long-ge, ZHANG Xin-fang. Breaking thermodynamic and kinetic barriers in superalloy homogenization process by electropulsing to improve mechanical properties [J]. Journal of Alloys and Compounds, 2021, 873: 159854.

[9] LI Yu-shuo, DONG Yan-wu, JIANG Zhou-hua, YAO Ke-an, DU Shu-yang, LIU Yu-xiao, HOU Zhi-wen. Study on microsegregation and homogenization process of a novel nickel-based wrought superalloy [J]. Journal of Materials Research and Technology, 2022, 19: 3366−3379.

[10] DU Jing-hui, LV Xu-dong, DONG Jian-xin, SUN Wen-ru, BI Zhong-nan, ZHAO Guang-pu, DENG Qun, CUN Chuan-yong, MA Hui-ping, ZHANG Bei-jiang. Research progress of wrought superalloys in Chian [J]. Acta Metallurgica Sinica, 2019, 55: 1115−1132.

[11] ZHANG Bei-jiang, ZHAO Guang-pu, ZHANG Wen-yun, HUANG Shuo, CHEN Shi-fu. Investigation of high performance disc alloy GH4065 and associated advanced processing techniques [J]. Acta Metallurgica Sinica, 2015, 51: 1227−1234.

[12] ZHANG Bei-jiang, HUANG Shuo, ZHANG Wen-yun, QING Tian, CHEN Shi-fu. Recent development of Nickel-based alloys and corresponding cast-wrought processing techniques [J]. Acta Metallurgica Sinica, 2019, 55: 1095−1114.

[13] HEGDE S R, KEARSEY R M, BEDDOES J C. Designing homogenization−solution heat treatments for single crystal superalloys [J]. Materials Science and Engineering, 2010, 527: 5528−5538.

[14] XIANG Xue-mei, JIANG He, DONG Jian-xin, YAO Zhi-hao. As-cast microstructure characteristic homogenization of a newly developed hard-deformed Ni-based superalloy GH4975 [J]. Acta Metallurgica Sinica, 2020, 56: 988−996.

[15] LI Hao-yu, DONG Jian-xin, LI Lin-han. Evolution of microstructure and hot deformation of GH4738 alloy during homogenization [J]. Transactions of Materials and heat Treatment, 2017, 38: 61−69. (in Chinese)

[16] LI Xin-xu, JIA Chong-lin, ZHANG Yong, LÜ Shao-min, JIANG Zhou-hua. Incipient melting phase and its dissolution kinetics for a new superalloy [J]. Transactions of Nonferrous Metals Society of China, 2020, 30: 2017−2118.

[17] YANG Hao-di, ZHOU Yang, LAI Yu, XIE Tao. Element segregation and homogenization process of 718Plus alloy ingot [J]. Transactions of Materials and Heat Treatment, 2021, 42: 69−75. (in Chinese)

[18] LIN Ying-ying, YU Qiu-ying, HE Xiao-yong, DONG Yun-peng, FANG Shuang, CHEN You-hong, ZHANG Min-cong. As-cast microstructure and homogenization process of difficult-to-deform GH4175 superalloy [J]. Transaction of Materials and Heat Treatment, 2021, 42: 54−60. (in Chinese)

[19] XIAO Dong-ping. Effect of homogenization treatment on hot deformation behavior of GH141 superalloy [J]. Transaction of Materials and Heat Treatment, 2022, 43(4): 107−115. (in Chinese)

[20] WANG Yi-lin, TAN Yi, LI Xiao-na, ZHAO Jia-qi, YOU Xiao-gang. Microsegregation and homogenization behavior of a Ni−Co based refractory superalloy for turbine dics [J]. Materials Characterization, 2023, 196: 112598.

[21] JABLONSKI P D, COWEN C J. Homogenizing a nickel-based superalloy: Thermodynamic and kinetics simulation and experimental results [J]. Metallurgical and Materials Transactions, 2009, 40: 182−186.

[22] RETTING R, RITTER N C, MULLER F, FRANKE M M, SINGER R F. Optimization of the homogenization heat treatment of nickel-based superalloy based on phase-field simulations: Numerical methods and experimental validation [J]. Metallurgical and Materials Transactions, 2015, 46: 5842−5855.

[23] ZHUANG Xin-peng, TAN Yi, ZHAO Long-hai, YOU Xiao-gang, LI Peng-ting, CUI Chuan-yong, Microsegregation of a new Ni−Co-based superalloy prepared through electron beam smelting and its homogenization treatment [J]. Journal of Materials Research and Technology, 2020, 9: 5422−5430.

[24] LI Xin-xu, JIA Chong-lin, ZHANG Yong, LÜ Shao-min,

JIANG Zhou-hua. Segregation and homogenization for a new nickel-based superalloy [J]. Vacuum, 2020, 177: 109379.
[25] SOHRABI M J, MIRZADEH H. Numerical and analytical solution for determination of interdiffusion coefficients in superalloys during homogenization [J]. Materials Today Communications, 2019, 21: 100631.
[26] YUE Xiao-dai, LI Jia-rong, SHI Zhen-xue, WANG Xiao-guang. Designing of the homogenization-solution heat treatment for advanced single crystal superalloys [J]. Rare Metal Materials and Engineering, 2017, 46: 1530−1535.
[27] ZHAO Long-hai, TAN Yi, WANG Yi-lin, YOU Xiao-gang, CHANG Kai, ZHUANG Xin-peng, LI Peng-ting, HU Ye-bing. Homogenization behavior of IN718 superalloy prepared by electron beam layered solidification technology [J]. Journal of Materials Research and Technology, 2021, 12: 1567−1575.
[28] SONG Wei-xi. Metallology [M]. 2nd ed. Beijing: Metallurgical Industry Press, 2008. (in Chinese)
[29] CHRISTIAN J W. The theory of transformations in metals and alloys [M]. 3nd ed. British Library Cataloguing, 2002.
[30] ZHOU Zi-jian, ZHANG Rui, CUI Chuang-yong, ZHOU Yi-zhou, SUN Xiao-feng. Effects of homogenization treatment on the microsegregation of a Ni−Co based superalloy produced by directional solidification [J]. Acta Metallurgica Sinica (English Letters), 2021, 34: 943−954.
[31] MIAO Zhu-jun, SHAN Ai-dang, WU Yuan-biao, LU Jun, XU Wen-liang, SONG Hong-wei. Quantitative analysis of homogenization treatment of Inconel718 superalloy [J]. Transactions of Nonferrous Metals Society of China, 2011, 21: 1009−1017.
[32] RAFIEI M, MIRZADEH H, MALEKAN M, SOHRABI M J. Homogenization kinetics of a typical nickel-based superalloy [J]. Journal of Alloys and Compounds, 2019, 793: 277−282.
[33] SEMIATION S L, KRAMB R C, TURNER R E, ZHANG F. Antony, Analysis of the homogenization of a nickel-base superalloy [J]. Scripta Materialia, 2004, 51: 491−495.
[34] MEI Shen-yong, ZHEN Lei, MENG Zhao-bin, ZHANG Mai-cang, DONG Jian-xin. Microsegregation and homogenization of GH105 superalloy ingot [J]. Journal of University of Science and Technology Beijing, 2009, 31: 714−718. (in Chinese)
[35] KRAMB R C, ANTONY M M, SEMIATIN S L. Homogenization of a nickel-base superalloy ingot material [J]. Scripta Materialia, 2006, 54: 1645−1649.
[36] JAVAD S M, HAMED M. Estimation of Homogenization time for superalloys based on a new diffusional model [J]. Materials Science and Technology, 2020, 36: 380−384.
[37] HILLERT M. Alloys diffusion and Thermodynamics [M]. Metallurgical Industry Press, 1984.

预测典型变形高温合金均匀化动力学的新模型

张献光[1,2]，杨文超[2]，周 扬[3,4]，闫建昊[2]，肖东平[3,4]，税 烺[3,4]，
付建辉[3,4]，孙 飞[5]，石 鹏[2]，陈佳俊[2]，裴逸武[2]，张 健[3,4]

1. 北京科技大学 绿色低碳钢铁冶金全国重点实验室，北京 100083；
2. 北京科技大学 冶金与生态工程学院，北京 100083；
3. 成都先进金属材料产业技术研究院股份有限公司，成都 610300；
4. 攀钢集团研究院有限公司，攀枝花 617000；
5. Department of Material Design Innovation Engineering, Nagoya University, Furo-cho, Chikusa-ku, Nagoya 464-8603, Japan

摘 要：提出一种基于扩散距离概念的变形高温合金均匀化动力学新预测模型。通过定量电子探针(EPMA)分析，系统研究典型镍基变形高温合金(GH4141)的微观偏析和均匀化动力学。研究发现，基于残余偏析指数模型预测的均匀化动力学与实际测量结果之间存在一定差异。实验和理论分析均表明，考虑了过去通常被忽略的扩散方向因子的一维扩散距离模型可以合理地预测均化动力学。新模型在只需知道原始枝晶臂间距和扩散系数前提下即可完成预测计算，这为变形高温合金均匀化动力学预测提供了一种新的选择。

关键词：变形高温合金；微观偏析；均匀化动力学；预测模型；扩散距离

(Edited by Bing YANG)